Supplementary Material for "Early Warning of mmWave Signal Blockage Using Diffraction Properties and Machine Learning"

Amirhassan Fallah Dizche, *Student Member, IEEE,* Alexandra Duel-Hallen, *Fellow, IEEE,* and Hans Hallen

In this supplementary document, we provide additional numerical results and derivations that are referred to in the paper.

S1. Simple Model Derivation

In this section, we present the derivation of the simple model. This simple model is used to provide insights into the Fresnel calculation results.

The oscillation patterns are obtained using the full Fresnel diffraction calculation [1] in the physical model with little insight as to their source. We can provide a rough, qualitative understanding of their origin by noting that finite element [2] calculations near a metal edge, which show the electric field distribution adjacent to the edge and thus indicate near-field sources for the Fresnel diffraction, exhibit a large electric field amplitude at the very edge. Thus, a qualitative approximation for the diffraction can be made by assuming that it generates a cylindrical passband wave $h_{edge}(t) = A_e/\sqrt{r(t)}\cos(\omega t - kr(t))$, with $r(t)$ the time-dependent distance from the blocker edge to the UE as in Fig. 1 of the main text, given by $r(t) = \sqrt{d^2 + v^2(t-t_t)^2 - 2dv(t-t_t)\sin(\alpha)}$ where $v = |\mathbf{v}|$, t_t is the time when the UE crosses the geometric transition, angular frequency $\omega = 2\pi f_c$, and $k = 2\pi/\lambda_c$. This wave is not a reflection, but an approximate near-field source for the Fresnel diffraction. It will interfere with the unscattered passband plane wave from the transmitter $h_T(t) = A\cos(\omega t - ku(t))$ traveling along the u-direction as shown in Fig. 1 of the main text, where $u(t) = d - v(t-t_t)\sin(\alpha)$. Thus, our simple model uses two plane waves propagating at an angle θ degrees with respect to each other as shown in Fig. 1 of the main paper. In general, two waves interfere to create a pattern with oscillation spatial period that ranges from $\lambda/2$ at $\theta = 180^\circ$ (opposite directions) to ∞ at $\theta = 0^\circ$ (co-propagating). Here, the angle θ between the two waves, hence the oscillation frequency, decreases as the geometric transition is approached. Along the geometric transition line, both plane waves propagate in the same direction. Beyond the transition, the plane wave from the BS is blocked, so only the cylindrical wave remains and thus interference (hence oscillation) stops.

We now derive an expression for this simple approximation for the oscillation prior to blockage to obtain an approximate RSS squared. Define the distance between the blocker edge and the receiver path where the path crosses the geometric LoS/NLoS transition (see Fig. 1 of the main paper) to be d. The angle α away from normal of the path crossing is also shown in Fig. 1 of the main paper. Let s denote a scalar distance from the UE to the geometric transition point along the path from LoS (x_0, y_0) to NLoS (x_1, y_1); it is negative in the LoS region, positive in NLoS.

The realistic physical model is based upon the coordinates (x, y) as shown in Fig. 1 of the main paper, but these are not optimal for deriving the simple model. Instead, we create a set of coordinates (u, q) by translating (x, y) so that the origin is at the blocker edge $\mathbf{r}_{bl}$, then rotate so that the coordinate u is along the geometric transition from the blocker as shown in Fig. 1 of the main paper. The coordinate q is perpendicular to u and also measured from the blocker but towards LoS. The distance from the (u, q) origin, $\mathbf{r}_{bl}$, to the mobile is $r = \sqrt{u^2 + q^2}$ (see Fig. 1 of the main paper). The interference between the two waves h_T and h_{edge} is given by the sum of the direct signal traveling along u and the cylindrical wave traveling along r. The cylindrical wave amplitude scales as $1/\sqrt{r}$. We also include a phase factor ϕ to account for the response of the scattering. The direct plane wave has amplitude A, and the amplitude of the cylindrical wave is thus $A_e = A\sqrt{d}$. Then the passband received signal corresponding to (1) in the paper is given by

$$\begin{aligned}\tilde{h}(u,v) =& A\,cos(\omega t - ku) + A\sqrt{d/r}\,cos(\omega t - kr + \phi)\\ =& A\,[cos(\omega t)\,cos(ku) + sin(\omega t)\,sin(ku) +\\ &+ \sqrt{d/r}\,cos(\omega t)\,cos(ku+\phi) +\\ &+ \sqrt{d/r}\,sin(\omega t)\,sin(ku+\phi)]\\ =& A\,cos(\omega t)\,[cos(ku) + \sqrt{d/r}\,cos(kr+\phi)] +\\ &+ A\,sin(\omega t)\,[sin(ku) + \sqrt{d/r}\,sin(kr+\phi)].\end{aligned}$$

From the above, the squared envelope of the equivalent lowpass signal is given by

$$\begin{aligned}h^2 =& A^2/2\,[cos^2(ku) + d/r\,cos^2(kr+\phi) +\\ &+ 2\sqrt{d/r}\,cos(ku)cos(kr+\phi) + sin^2(ku) +\\ &+ d/r\,sin^2(kr+\phi) + 2\sqrt{d/r}\,sin(ku)sin(kr+\phi)]\\ =& A^2/2\,[1 + d/r + \sqrt{d/r}\,cos(ku - kr - \phi)]\\ =& A^2/2\,[1 + d/r - \sqrt{d/r}\,cos(ku - kr)],\end{aligned}$$

where the last line assumes that $\phi = 180^\circ$ as expected and is consistent with the known result of $h^2 = A^2/2$ along the

This work was partially supported by National Science Foundation Grant ECCS-2122012.

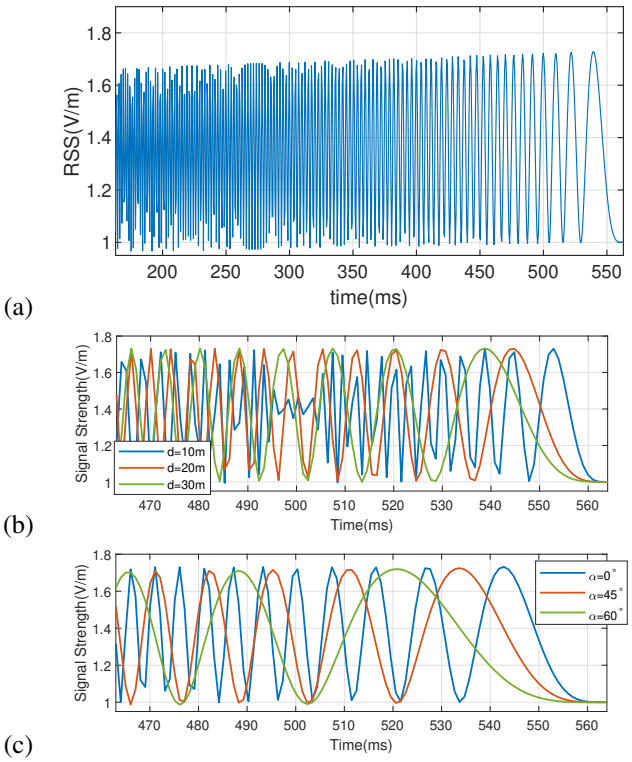

Fig. S1. Parameter variation calculations of the simple model for a 5 m path length ending at the geometric transition $s = 0$ with speed 28 m/s, the T_x at (x, y) = (-10, 0) m and the blocker at (0, 0) m so the (x, y) and (u, q) axes are the same. (a) Simple two-wave model. (b) Change d: $\alpha_1 = \alpha_2 = \alpha_3 = 0°; d_1 = 50m, d_2 = 30m, d_3 = 10m$. Compare to Fig. 4(a). (c) Change α: $\alpha_1 = 0°, \alpha_2 = 45°, \alpha_3 = 60°; d_1 = d_2 = d_3 = 40m$. Compare to Fig. 4(b).

geometric transition where $u = d = r$. This result is placed onto the path of the mobile in the LoS region (where s is negative),

$$u = d - s\,sin(\alpha);\;\; q = -s\,cos(\alpha)$$
$$r = \sqrt{d^2 - 2ds\,sin(\alpha) + s^2 sin^2(\alpha) + s^2 cos^2(\alpha)}$$
$$= \sqrt{d^2 + s^2 - 2ds\,sin(\alpha)}.$$

To convert to the parameters of the main paper, we rewrite the mobile path parameter s as $s = -v(t - t_t)$ where here the speed is v and referenced to a time t_t when the UE crosses the geometric transition. Inserting this into the above, we obtain

$$|h(t)|^2 = A^2/2\,(1 + d/r(t) - \sqrt{d/r(t)}\,\cos(ku(t) - kr(t)),$$

where we emphasize that u and r are time-dependent via substituting for s: $u = d - v(t - t_t)\,sin(\alpha)$ and $r = \sqrt{d^2 + v^2(t - t_t)^2 - 2dv(t - t_t)\,sin(\alpha)}$.

Figure S1(a) shows the result for the scenario of Figs. 1 and 2 of the main paper. The simple model explains most of the qualitative features of the oscillation pattern, including frequency change and the variation with angle α and distance d. In Fig. S1(a), we observe the reduction in the oscillation pattern envelope with time (distance) from $t_t = 563(ms)$ (geometric transition crossing) as t decreases, i.e., $t_t - t$ grows. While the $1/\sqrt{r(t)}$ dependence of the cylindrical wave $h_{edge}(t)$ could explain this decrease, the latter effect is much less pronounced than in the pattern of Fig. 2 of the main paper, which is generated using a full diffraction calculation. This discrepancy is likely caused by the approximations of the simple model (1). In fact, the simple model also fails in the NLoS region. Contributions from regions away from the edge (in the full Fresnel formalism of our realistic physical model) are needed to properly match the actual signal. Thus, we do not use the simple model for any training or testing scenario creation (the realistic physical model is used for those cases). Results in Fig. S1 can be compared to the Figs. 4(a-c) in the main text. The simple model is useful for insights into the origins of several key properties of the pattern used for early warning.

S2. ML Evaluation Metrics and Complexity

The four possible outcomes for the prediction problem are: true positive (TP), true negative (TN), false positive (FP), and false negative (FN) where the symbols TP, TN, FP, and FN represent the total number of corresponding outcomes for the test dataset (D_j). We use the following performance metrics for this analysis: accuracy= $\frac{\text{TP+TN}}{\text{TP+TN+FP+FN}}$, f1 score= $\frac{\text{TP}}{\text{TP+0.5(FP+FN)}}$, and area under the curve (AUC), defined as the area under the receiver operating curve (ROC), which plots $\text{TPR} = \frac{\text{TP}}{\text{TP+FN}}$ vs $\text{FPR} = \frac{\text{FP}}{\text{FP+TN}}$ [3].

To study the effect of size of the dataset $\mathcal{D}$ on EW performance, we vary N from 1000 to 100,000 and report the EW accuracy, f1 score, and AUC for each case. Table S1 summarizes the simulation results. We observe that for $N < 10,000$ the EW performance degrades while increasing N over 10,000 does not change the EW performance significantly. Therefore, $N = 10,000$ is a suitable size for dataset $\mathcal{D}$. Similar conclusions were reached for other prediction times t_s, P, as well as multipath fading and noisy data.

TABLE S1
EW performance vs dataset size N, $W = 400(ms)$, $f_s = 1$kHz, $t_1 = 250(ms)$, $P = 50(ms)$, dataset $\mathcal{D}$

N	Accuracy	f1 score	AUC
1000	89.74%	0.8259	0.8712
3000	97.87%	0.9641	0.9641
6000	98.86%	0.9793	0.9839
10000	99.53%	0.9919	0.9955
20000	99.60%	0.9928	0.9972
100000	99.61%	0.9928	0.9972

Finally, in our experiments for $N = 10,000$, physical model dataset generation, offline training, and testing take $1179(s)$, $62(s)$, and $0.69(s)$, respectively, for each EW result in Table I of the main paper, demonstrating low computational complexity of the proposed ML method. Moreover, it takes $0.34(ms)$ to compute the EW result in real time, which is negligible compared to the prediction range of hundreds of milliseconds. The experiments are run using Python on a PC with 3.4 GHz Intel core-i7 processor and 16 GB of memory.

S3. Performance for Fading Signals

The results of the experiment discussed in Section IV, paragraph 2 and Table I of the paper for fading dataset $\mathcal{D}_f$

is reported in Table S2. Moreover, an example of a smoothed fading signal from dataset $\mathcal{D}_f$, sampled at 6KHz and passed through an L1 moving average filter with window size of 60 is shown in Fig S2. ML performance for the resulting smoothed fading signal dataset $\mathcal{D}_s$ are reported in Table S3.

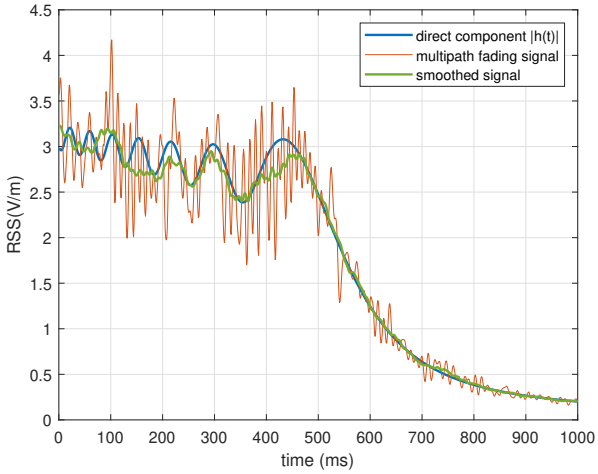

Fig. S2. RSS $|h(t)|$ for noiseless signal, multipath fading signal, and smoothed signal, transitioning from LoS to NLoS.

S4. Effect of Speed on Early Warning

Additional statistics including the f1-score and AUC of the experiments described and presented in Table II of the main paper are shown in Table S4. We observe that the f1-score and AUC follow the same trends as the accuracy reported in Table II of the paper.

S5. Performance metrics for noisy and fading measurements

Additional simulation for the f1-score and AUC of the experiments described in the last paragraph of Section IV in the paper are provided in Fig. S3

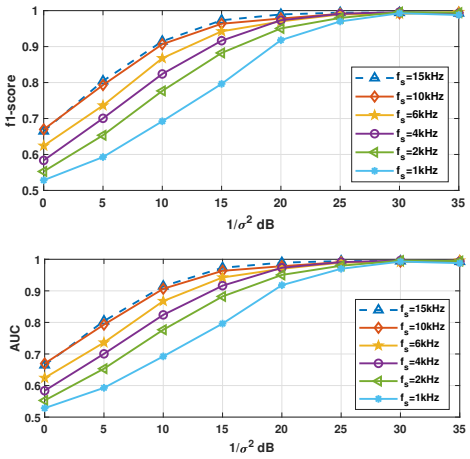

Fig. S3. F1 score and AUC of mmWave EW of blockage of multipath fading signal dataset $\mathcal{D}_f$ vs $1/\sigma^2$ for $f_s = \{1, 2, 4, 6, 10, 15\}$ kHz, $W = 400(ms)$, $t_1 = 250(ms)$ and $P = 50(ms)$. See Fig. 6 in the paper.

References

[1] Guenther, Robert D., *Modern Optics*, 2nd ed. Oxford, New York: Oxford University Press, Jun. 2018.

[2] C. Multiphysics, "Introduction to comsol multiphysics®," *COMSOL Multiphysics, Burlington, MA, accessed Feb*, vol. 9, p. 2018, 1998.

[3] C. M. Bishop and N. M. Nasrabadi, *Pattern recognition and machine learning*. Springer, 2006, vol. 4, no. 4.

TABLE S2
ACCURACY (%) OF ML-BASED EW OF BLOCKAGE METHOD; FADING RECEIVED SIGNAL, $W = 400(ms)$, RICIAN FADING, K=11dB, SAMPLING RATE f_s IS SHOWN IN THE TOP ROW.

P(ms)	t1(ms)	1kHz	2kHz	4kHz	6kHz	10kHz	15kHz
10	$100-250$	85.79	86.01	86.48	87.45	88.94	89.09
10	450	80.33	81.58	82.69	84.52	85.06	85.79
10	550	71.57	73.33	76.35	81.09	83.12	83.27
25	$100-250$	97.31	97.49	97.96	98.27	98.54	98.94
25	450	95.24	95.27	95.28	95.30	95.56	95.73
25	550	91.97	91.98	91.97	91.97	91.97	92.28
> 50	$100-250$	99.53	99.54	99.56	99.59	99.61	99.63
> 50	450	97.07	97.07	97.07	97.07	97.08	97.22
> 50	550	94.39	94.39	94.41	94.43	94.88	94.90

TABLE S3
ACCURACY (%) OF ML-BASED EW OF BLOCKAGE METHOD; FADING RECEIVED SIGNAL FIRST SAMPLED AT 6KHZ AND THEN PASSED THROUGH AN L1 MOVING AVERAGE FILTER WITH WINDOW SIZE OF 60, $W = 400(ms)$, RICIAN FADING, K=11dB. SUB-SAMPLING RATE f_s IS SHOWN IN THE TOP ROW.

P(ms)	t1(ms)	1kHz	2kHz	4kHz	6kHz	10kHz	15kHz
10	$100-250$	84.22	85.47	86.22	86.93	87.21	87.99
10	450	79.75	80.58	81.29	93.67	84.26	84.93
10	550	70.89	72.59	75.74	80.56	82.81	82.54
25	$100-250$	96.67	96.57	97.07	97.97	98.42	98.76
25	450	94.68	94.57	95.13	95.27	95.44	95.67
25	550	90.73	90.98	91.08	91.57	91.66	92.02
> 50	$100-250$	99.09	99.14	99.28	99.33	99.41	99.44
> 50	450	96.67	96.99	97.01	97.01	97.02	97.03
> 50	550	93.93	93.98	94.01	94.01	94.02	94.02

TABLE S4
F1-SCORE AND AUC OF ML-BASED EW OF BLOCKAGE METHOD; MULTIPATH FADING (F) AND NON-FADING(NF) DATASETS, $W = 400(ms)$, $t_1 = 250(ms)$, $P = 50(ms)$; RICIAN FADING, K = 11 dB. FOR $f_s \leq 200Hz$, FADING SIGNALS ARE L1 FILTERED USING SAMPLING RATE = 6KHZ, WINDOW SIZE = 60.

	$f_s \rightarrow$	1 KHz		200 Hz		100 Hz		50 Hz	
	speed (m/s) $\downarrow$	NF	F	NF	F	NF	F	NF	F
f1-score	0-5	0.9989	0.9981	0.9707	0.9595	0.9685	0.9573	0.9621	0.9509
	5-10	0.9940	0.9925	0.9624	0.9490	0.9579	0.9445	0.9509	0.9375
	10-15	0.9933	0.9915	0.9457	0.9300	0.9422	0.9265	0.9311	0.9154
	15-20	0.9901	0.9887	0.9149	0.8858	0.9108	0.8817	0.9092	0.8801
	20-25	0.9883	0.9879	0.8579	0.8266	0.8503	0.8190	0.8404	0.8091
	25-30	0.9855	0.9849	0.7768	0.7410	0.7605	0.7247	0.7520	0.7162
AUC	0-5	0.9947	0.9932	0.9786	0.9674	0.9711	0.9599	0.9618	0.9506
	5-10	0.9918	0.9909	0.9664	0.9530	0.9526	0.9392	0.9499	0.9365
	10-15	0.9901	0.9898	0.9526	0.9369	0.9505	0.9348	0.9325	0.9168
	15-20	0.9854	0.9854	0.9297	0.9006	0.9258	0.8967	0.9155	0.8864
	20-25	0.9834	0.9833	0.8651	0.8338	0.8557	0.8244	0.8547	0.8234
	25-30	0.9820	0.9815	0.7802	0.7444	0.7729	0.7371	0.7601	0.7243